

RESEARCH ARTICLE

Harmonics Mitigation Filter for High-Power Applications

ALI SUNBUL^{1,2}, (Student Member, IEEE),
ABDULRAHMAN ALDURAIBI^{1,3}, (Member, IEEE), AND FIRUZ ZARE^{1,4}, (Fellow, IEEE)

¹School of Information Technology and Electrical Engineering, The University of Queensland, Brisbane, QLD 4072, Australia

²Department of Electrical Engineering, College of Engineering, Taibah University, Yanbu 46421, Saudi Arabia

³Department of Electrical Engineering, College and Engineering, Qassim University, Unaizah 56452, Saudi Arabia

⁴School of Electrical Engineering and Robotics, Queensland University of Technology, Brisbane, QLD 4000, Australia

Corresponding author: Ali Sunbul (a.sunbul@uq.net.au)

The work of Ali Sunbul was supported by Taibah University, Medina, Saudi Arabia, through Saudi Arabian Cultural Mission in Australia.

ABSTRACT This research work proposes a cost-effective Hybrid Active Harmonic Filter (HAHF) method to mitigate current harmonics in an industrial or commercial power network. The proposed HAHF is based on a Silicon-Controlled Rectifier with an Electronic Inductor (SCR-EI) topology with a reduced number of fully active switches and a better harmonic performance. A new shifted-pulse current modulation method is proposed to cancel harmonics caused by other converters. A Particle Swarm Optimisation (PSO) algorithm is implemented to optimise the modulation parameters and minimise the total harmonics. A lab prototype is implemented in the laboratory to validate the proposed mathematical method and simulation results.

INDEX TERMS Active power filter, adjustable speed drives (ASD), harmonic mitigation, hybrid active harmonic filter, selective harmonic cancellation, power electronics, PSO algorithm.

I. INTRODUCTION

The utilisation of power electronic converters on the electrical distribution network has rapidly increased in the last decades. Although these power electronic converters have increased the controllability and efficiency of electrical systems, they may be a major source of current harmonics and decay the performance of all devices connected to the electrical grid [1]. Strict standards have been introduced, such as IEEE 519, to minimise the negative influence of current harmonics on the systems connected to the distribution network [2].

Several topologies have been utilised to reduce the current Total Harmonic Distortion (THD_i), such as transformer-based multi-pulse rectifiers, electronic transformer-based rectifiers, and active rectifiers. For the multi-pulse rectifiers, 12-pulse, 18-pulse, 24-pulse, and 30-pulse rectifiers are employed in [3], [4], [5], and [6]. Although the multi-pulse rectifiers improve the THD_i, it requires bulky and lossy shifting transformers, while the relationship between the THD_i and the number of pulses is not linear. In addition, the electronic transformer-based rectifiers are employed in [7] and [8]

The associate editor coordinating the review of this manuscript and approving it for publication was Zhuang Xu¹.

to reduce the THD_i, but they require a higher number of parallel units to further reduce the harmonics and require a proper controller for current sharing. On the other hand, active rectifiers are utilized in [9] to shape close to sinusoidal currents with low THD_i, but they are expensive and complex to control. Although all the above-mentioned topologies contribute to reducing the injected THD_i to the grid, they are not able to selectively cancel the existing harmonics on the grid or electrical distribution network.

In the literature, there are two main categories of filters to reduce the current harmonics of the distribution network, which are passive and active filters. Passive filters utilise a combination of passive elements, such as inductors, capacitors, and/or resistors, to reduce the current harmonics. However, passive filters' performance depends on the load, and their components' values are subject to change with temperature and time. They are also susceptible to their tuning. Therefore, generating resonance is a significant problem, and this category of filters is undesirable [10].

Active harmonic filters or active power filters utilise active switching devices, such as Insulated Gate Bipolar Transistor (IGBT). They provide superior performance and overcome the aforementioned issues of passive filters [11],

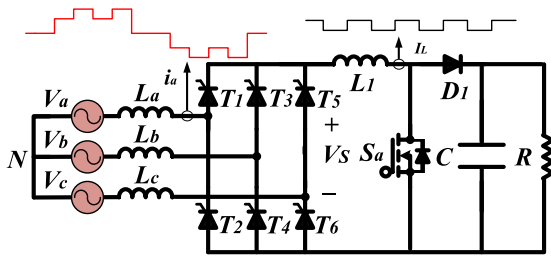


FIGURE 1. The Hybrid Active Harmonic Filter (HAHF) topology based on SRC-EI.

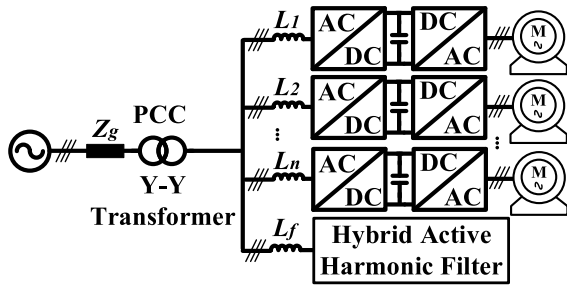


FIGURE 2. The Adjustable Speed Drives (ASD) with the Hybrid Active Harmonic Filter (HAHF).

[12], [13], [14]. This type of filter is divided into a pure active filter and a hybrid active filter. The Hybrid Active Harmonic Filter (HAHF) employs a combination of passive and active switching devices. Pure active filters are relatively expensive for high-power applications, making them less attractive [15].

On the other hand, hybrid active filters are preferable because of their cost-effectiveness [16], [17], [18], [19]. Several hybrid harmonic filters have been proposed in the literature [20]. The control method for these filters is essential to select the specific harmonics to be mitigated and maintain the power quality level [21], [22], [23].

In [24], a HAHF employs six active switches connected in series with a passive filter. This topology is proposed to reduce the power rating and improve the power quality. On the other hand, another HAHF with superior performance and a reduced number of switches (four switches) is proposed in [25], [26], and [27]. Numerous research articles have been proposed on this topic, which contributed to the advancement of the active harmonic filter's technology. Although these filters are technically matured, the commercially available active filters are still unrealistic practical solutions due to their high cost, especially for high-power applications, such as three-phase Adjustable Speed Drives (ASD) [28].

The international standards permit ASD systems to have relatively high Total Current Harmonics (THDi) based on [29]; hence, a diode bridge rectifier is still preferred in industrial ASD applications. An Electronic Inductor (EI) based on a boost converter integrated with Diode Rectifier (DR) is proposed to improve the current harmonics and maintain a constant power quality despite the variation in the load [30]. Moreover, a current modulation technique for the DR-EI is proposed in [31], [32], [33], [34], and [35] to mitigate specific harmonics. This current modulation technique is

also utilised in a combination of DR-EI and parallel Silicon Controlled Rectifiers (SCR) with EI to improve the current harmonics [36], [37], [38].

The aforementioned research aims to mitigate harmonics at the unit level of ASD. On the other hand, [39] proposed a method based on DR-EI topology to mitigate harmonics on the ASD distribution network selectively; however, this method cannot reduce more than one harmonic simultaneously, and the THD_i is still relatively high. In this research, a modified shifted pulse current modulation technique based on an SCR-EI topology shown in Fig. 1, with superior performance, is proposed to mitigate current harmonics on the industrial or commercial power network. In other words, this paper proposes an economical solution for a HAHF suitable for high power applications (ASD) with a reduced number of active switches (only one fully active switch). The proposed system utilises SCR due to its design simplicity, ruggedness, efficiency, low cost, and high voltage and current capability, which makes it suitable for high-power applications [40]. In fact, SCRs are widely employed for high-power applications, such as motor drives and wind power generation applications [41], [42]. The proposed system aims to control the magnitude and phase angle of any order of current harmonics in the distribution network. A genetic optimisation algorithm, known as Particle Swarm Optimization (PSO) [43], is employed to optimize the parameters of the proposed shifted pulse modulation technique. The proposed system can be placed at the Point of Common Coupling (PCC) to actively eliminate harmonics, as depicted in Fig. 2; however, in this research, an ASD with a three-phase front-end DR is considered as a case study of grid harmonics. A summary of the novelties presented in this paper is as follows:

- A modified pulse-shaped harmonic mitigation method based on SCR-EI is proposed.
- A PSO optimisation algorithm to minimise the harmonic contents at the PCC is implemented.
- Comprehensive experimental testing is performed to validate the proposed HAHF.

This research is organised as follows. Harmonic analysis for the electrical distribution system of conventional ASD systems is illustrated in Section II. Then, the proposed shifted pulse current modulation technique is explained in Section III. The details of the PSO algorithm are provided in Section IV. Section V presents the details of the hardware implementation of the proposed system, while section VI depicts the results of the system. Finally, the conclusion is included in Section VII.

II. HARMONICS ANALYSIS FOR ELECTRICAL DISTRIBUTION NETWORK

The first step to mitigating harmonics from the electrical distribution system is to identify the magnitude and phase angle of the current harmonics at the PCC. Then, the active harmonic filter generates a waveform that minimises the targeted harmonics of the electrical distribution network. In this paper,

an Adjustable Speed Drive (ASD) distribution network is selected as a case study. The ASD distribution network is chosen since they are the major load in today's global electrical grid. Since most industrial ASD systems are still employing conventional DR, harmonics analysis for DR-based ASD is provided. Generally, the ASD distribution network can have single or multiple drives.

In this research, the harmonic contents of the electrical distribution network are analysed in two different scenarios. The first scenario is when only a single DR-based ASD is connected to the grid, while the second scenario is when the electrical grid supplies twenty DR-based ASD. The impact of having a single or twenty drives on the harmonic contents of the distribution network is analysed in [39] and illustrated in Table 1. In other words, the harmonics generated by a single and twenty ASD systems are investigated. However, the differences in the current harmonics' magnitude and phase angle at the PCC are compared in this section. Table 1 depicts the magnitude and phase angle of major current harmonics injected into the grid when twenty DR-based ASD systems or a single DR-based ASD system is connected to the grid. It is illustrated from the table that the magnitudes of the harmonics are generally similar for single and multiple ASD systems. However, the 7th harmonic in the single ASD is more than 15 % higher than in multiple ASD. The reason for that is when multiple ASD systems are connected at the same PCC; some harmonics may be cancelled depending on the power level of each drive.

TABLE 1. Current harmonics generation from single and twenty ASD systems based on diode rectifiers.

ASD System's Harmonics	Single Drive System	Twenty Drives System
i_5	36.1%	32.1%
θ_5	125°	122°
i_7	26.5%	11.3%
θ_7	240°	208°
i_{11}	8.9%	7.5%
θ_{11}	3°	288°
i_{13}	8.4%	4.2%
θ_{13}	28°	310°
THD _i	48%	35.5%

There are also variations in the harmonics phase angle for single and multiple ASD systems. For example, the 7th, 11th, and 13th have phase angle variations of 32°, 75°, and 78°, respectively, at full power operation. On the other hand, the phase angle variation for the 5th harmonic is neglectable.

Obviously, the values of the current harmonics are different in the single drive and multiple drive systems; however, the differences are insignificant when investigating the harmonic cancellation technique. Indeed, the comparison results demonstrate that the single ASD system is the worst-case scenario since it has a higher THD_i; hence, the single ASD

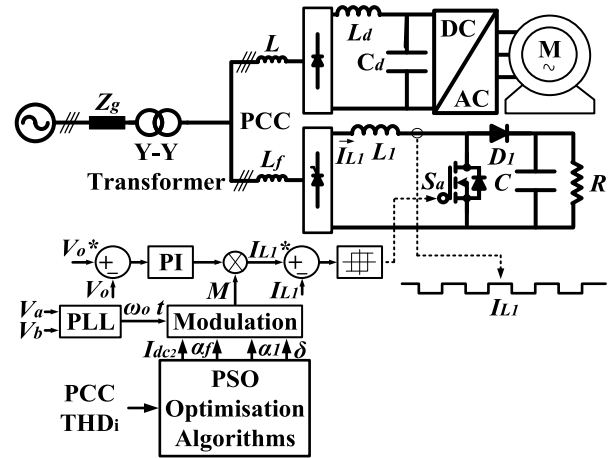


FIGURE 3. The scheme of the proposed system.

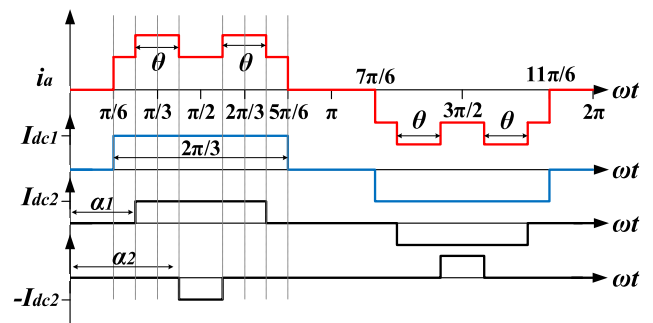


FIGURE 4. The waveforms of the conventional modulation method.

system (conventional DR with passive filter) is utilised as a case study to represent the loads in the grid. Despite the differences between the magnitude and phase angle of harmonic values produced by the DR with passive filter and the multiple ASD systems, this paper aims to prove that the proposed technique is capable of producing harmonics with a desired magnitude and phase angle to cancel harmonics from the PCC.

Fig. 3 depicts the configuration of the implemented proposed system. The system consists of an ASD with a front-end three-phase DR with a passive filter, as a case study of grid harmonics, and a parallel HAHF.

III. SHIFTED PULSE CURRENT MODULATION TECHNIQUE FOR THE ELECTRONIC INDUCTOR (EI)

Modifying the dc current of the boost-based EI (I_L) leads to direct control of the input AC current (i_a , i_b , and i_c); hence, the dc current (I_{dc1}) can be modulated to mitigate current harmonics at the grid's PCC.

A. CONVENTIONAL METHOD

The current modulation technique proposed in [31] is composed of a summation of three waveforms, as illustrated in Fig. 4. The first one (I_{dc1}) represents the conventional DR-EI current waveform conducting for 120 degrees due to the diode bridge limitation. The individual harmonic of this square

wave is found by the Fourier series as written in (1):

$$i_n = \frac{4I_{dc1} \cos(30n)}{n\pi} \quad (1)$$

The second and third waveforms (I_{dc2} and $-I_{dc2}$) are the modulated current from boost-based EI. The results from these three waveforms shape the grid current. The input current (i_a) has a stepped-shaped waveform. The first current level starts at ($t = \pi/6$); then, the current is controlled to move to the second level at ($t = \alpha_1$). Finally, the current goes back to the first level from ($t = \alpha_2$) until ($t = \pi/2$). From time equal to ($t = \pi/2$) until ($t = 5\pi/6$), the same pattern is repeated. The individual harmonic of this new waveform (coloured in red) is found by the summation of the three waveforms' harmonics as shown in (2) [31]:

$$i_n = \frac{4I_{dc1} \cos(30n)}{n\pi} + \frac{4I_{dc2} \cos(n\alpha_1)}{n\pi} - \frac{4I_{dc2} \cos(n\alpha_2)}{n\pi} \quad (2)$$

The parameters I_{dc2} and α_1 should be optimised to reach the optimal harmonics reduction.

The red waveform shown in Fig 4 illustrates that the centre of the second level pulse is always fixed at ($t = \pi/3$). In contrast, the width of the pulse, noted by θ , can be controlled to achieve the desired harmonic mitigation. The result of this method enables low-order harmonics cancellation with a slight improvement in the THD_i. The drawback of this method is the limitation of the conduction period from time equal $\pi/6$ to $5\pi/6$ and the lack of controlling the center of the second pulse I_{dc2} .

B. SHIFTED PULSE METHOD

Instead of the centralised pulse in part 3, a shifted pulse current modulation technique for the DR-EI is proposed in [39], as depicted in Fig. 5. This technique is similar to the conventional technique in part A. However, the only difference is that the centre of the pulse is shifted from ($t = \pi/3$) by a value of (δ). The individual harmonic of this current is found in (3) [39]:

$$i_n = \frac{4I_{dc1} \cos(30n)}{n\pi} \perp 0 + \frac{4I_{dc2} (\cos(n\alpha_1) - \cos(n\alpha_2))}{n\pi} \perp -(n\delta)\theta \quad (3)$$

In this technique, the I_{dc2} , α_1 , and δ need to be optimised for harmonics reduction. When this method is implemented with the conditional DR at full-power operation, the THD_i reduces from 48% to 36%. Although this technique has the advantage of controlling the second pulse I_{dc2} , it has a limitation in controlling the first pulse I_{dc1} .

C. PROPOSED SHIFTED PULSE METHOD

In order to increase the capability of the hybrid harmonics filter in the literature, a modified shifted pulse current modulation technique based on Silicon-Controlled Rectifier (SCR) with EI topology (SCR-EI) is proposed as shown in

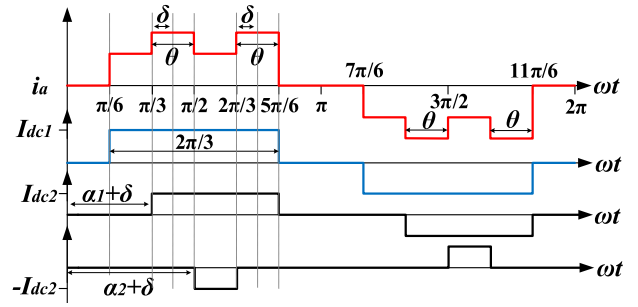


FIGURE 5. The waveforms of the Shifted-pulse modulation method.

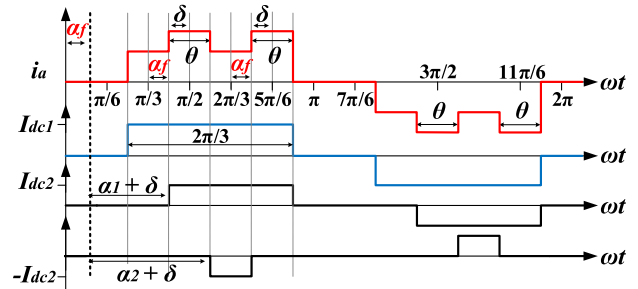


FIGURE 6. The waveforms of the proposed Shifted-pulse modulation method.

Fig. 3. The proposed technique is capable of mitigating a wider range of harmonics as compared to the pre-existing technique. Similar to parts 1 and 2, the mains current is a summation of three waveforms, as illustrated in Fig. 6. The maximum conduction period is still limited to 120 degrees because of the nature of the SCR bridge rectifier. However, when the SCR-EI is employed in parallel with ASD systems, it can increase the system's overall conduction period. The starting point of the current conduction (I_{dc1}) is not fixed at ($t = \pi/6$) but controlled by a variable (α_f), and the new starting point is ($t = \alpha_f + \pi/6$), which leads to shifting the centre of the pulse (I_{dc1}). In the proposed method, the centre of the second pulse (I_{dc2}) is controlled by two parameters (δ and α_f), and the new centre of the pulse is equal to ($t = \pi/3 + \delta + \alpha_f$). In comparison, the pulse's centre is fixed at ($t = \pi/3$) in the conventional method while controlled to be equal to ($t = \pi/3 + \delta$) in the shifted pulse method. Hence, the current conduction starting point (α_f), the pulse's magnitude (I_{dc2}), pulse's starting point (α_1), and centre (δ) are controlled to mitigate current harmonics in the electrical distribution network. The individual harmonic, in this method, is proposed in (4).

$$i_n(t) = \frac{4I_{dc1}}{n\pi} \cos\left(n\frac{\pi}{6}\right) \sin(n\omega t - n\alpha_f) + \left[\frac{4I_{dc2}}{n\pi} \cos(n\alpha_1) - \frac{4I_{dc2}}{n\pi} \cos(n\alpha_2) \right] \times \sin(n\omega t - n\alpha_f - n\delta) \quad (4)$$

Conditions (5) must be met at all times to avoid unwanted harmonics and guarantee symmetrical AC currents.

$$i_a + i_b + i_c = 0 \quad (5)$$

The limitation or boundaries of α_1 is constructed based on the standard waveform in Fig 4. In other words, both shifting parameters (α_f and δ) are assumed to be zero when selecting α_1 . Since α_1 is the starting point of the second-level pulse conduction period, it must be larger than the starting point of the first-level pulse (30°) and smaller than the centre of the second-level pulse (60°), as illustrated in (6); to ensure symmetrical 3-phase current waveforms

$$30 \leq \alpha_1 \leq 60 \tag{6}$$

The pulse's width (θ) and α_2 can be directly derived from α_1 ; hence, optimising α_1 means α_2 and θ are optimised. The parameters are calculated in the following:

$$\alpha_2 = 120 - \alpha_1 \tag{7}$$

$$\theta = 2(60 - \alpha_1) \tag{8}$$

The shift of the second-level pulse (δ) is dependent on the selected α_1 , as illustrated in (9).

$$30 - \alpha_1 \leq \delta \leq -30 + \alpha_1 \tag{9}$$

In general, the firing angle of the SCR is limited to 180° . However, it is limited to 60° in this application to limit the increment of the displacement factor and ensure that the input voltage of the EI is sufficiently high to operate in CCM. Hence, the firing angle (α_f) is limited, as shown in (10).

$$0 \leq \alpha_f \leq 60 \tag{10}$$

The derived equation (4) is a summation of three waveforms, as illustrated in Fig 6. The first waveform is a pulse that has a magnitude of (I_{dc1}) with a fixed width of 120° (at limited α_f) and a variable centre depending on the firing angle (α_f). The second and third waveforms have a magnitude of I_{dc2} and $-I_{dc2}$, respectively. The width of the second waveform is dependent on both the firing angle (α_f) and the variable (α_1), while the centre is dependent on the variable (δ). Finally, the centre of the third waveform is the same as the second waveform's centre, while the width is a consequence of the selection of (α_1). The concept behind the dependency of the third waveform on the second waveform is to ensure that the three-phase currents are symmetrical.

The proposed equation (4) can be generalised by an m-number of levels, as shown in (11) and illustrated in Fig 7.

$$i_n(t) = \frac{4I_{dc1}}{n\pi} \cos\left(n\frac{\pi}{6}\right) \sin(n\omega t - n\alpha_f) + \frac{4}{n\pi} \times \left[\sum_{i=2}^m \cos(n\alpha_{ia}) - \frac{4I_{dc2}}{n\pi} \cos(n\alpha_{ib}) \right] \times \sin(n\omega t - n\alpha_f - n\delta) \tag{11}$$

The manipulation of the pulse's parameters allows the proposed filter to generate harmonics similar to the distribution system's harmonics in magnitude but with the opposite phase angle. Thus, the harmonics are reduced. When implementing this proposed method with a conventional DR, the THDi significantly reduces. In this research, an optimisation algorithm is built to select the proper pulse parameters, as explained next section.

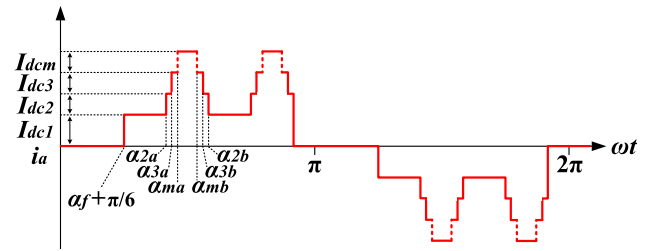


FIGURE 7. The waveforms of the proposed Shifted-pulse modulation method with m-number of levels.

IV. IMPLEMENTATION OF PARTICLE SWARM OPTIMISATION (PSO) ALGORITHM

The basic principle of optimisation is to explore all available solutions, evaluate them, then provide the optimum set of solutions. In other words, the optimization algorithm finds suitable combinations of pulse parameters (I_{dc2} , α_f , α_1 , δ) that results in the optimised harmonic level. The designer specifies the constraints (K_n) or upper limit of the targeted harmonics, and the optimization algorithm finds a suitable set of parameters that result in acceptable harmonic content (h_n). The n^{th} harmonic content and its constraint are shown in (12).

$$h_{SYSn} = |i_n + i_{PCCn}| \leq K_n, \tag{12}$$

where $n = 5, 7, 11, 13, \dots, n_{max}$

In (12), i_{PCCn} is the n^{th} harmonic content at the PCC (without applying active harmonic mitigation), while h_{SYSn} is the n^{th} harmonic content at the PCC (active harmonic mitigation is applied). i_n is the n^{th} harmonic content of the HAHF, which can be calculated using (4). The constraint (K_n) is chosen based on the maximum permissible harmonic level by the application.

The objective is to minimise the individual harmonics to achieve acceptable harmonics by the grid and reduce the THDi. In order for the optimiser to evaluate the pulse's set of parameters, an objective function must be derived. Equation (13) illustrates the system's objective function that needs to be minimised. It consists of the summation of the individual harmonic (h_{SYSn}) multiplied by a factor (WF_n), which prioritises the significant harmonics.

$$F_{obj} = \sum_{n=1,5,7,11,13,\dots}^{n_{max}} WF_n h_{SYSn} \tag{13}$$

Particle Swarm Optimisation (PSO) is a stochastic Genetic Algorithm (GA) that was first proposed in 1995 by Kennedy and Eberhard. The basic idea of PSO is inspired by the swarm intelligence of real-life creatures such as birds, fish, and ants. The main advantages of PSO are the easy implementation, fast convergence, and capability of escaping local optimum. The swarm particles collaborate and share information to achieve their goals in a fast manner. The number of particles is identified by the designer. These particles search together in the search space to find the best solution. Each member of the swarm flying around the search space is identified by its current position and velocity. They are capable of remembering their best position. Each particle has its own velocity,

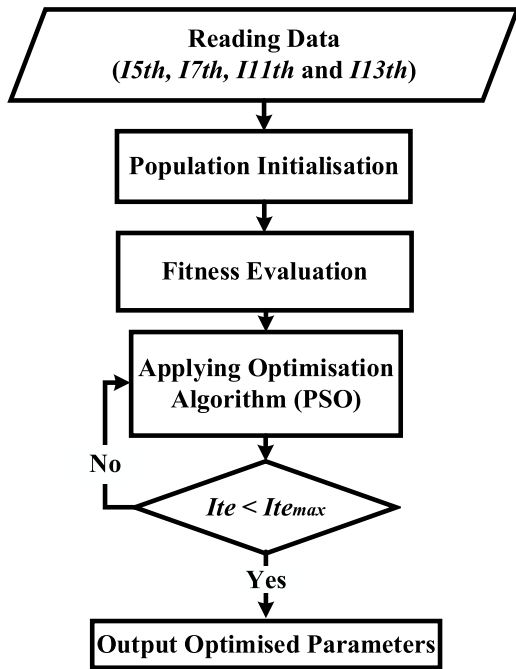


FIGURE 8. The General Scheme of the PSO algorithm.

which identifies the direction of its next position. The value of velocity is influenced by both the particle’s personal best position and the global best position of all particles.

Figure 8 depicts the implementation of the PSO algorithm in the Hybrid Active Harmonic Filter (HAHF) system. The implementation follows the following steps:

1) READING DATA

The harmonics that need to be mitigated from the distribution network are imported.

2) INITIATING THE OPTIMISATION POPULATION AND PARAMETERS

The optimisation parameters are set, and the initial population is produced using a uniformly random initialisation technique.

3) APPLYING THE PSO ALGORITHM

The particles’ position and velocity are updated to reach the optimum current waveform, which minimises the distribution network’s harmonics.

4) CHECKING THE TERMINATION CONDITION

The number of iterations is checked; if the maximum number of iterations (ite_{max}) is reached, the algorithm will output the optimum solution. On the other hand, step 3 will be repeated if the maximum number of iterations is not reached.

In PSO, the population of the swarm (NP) is chosen by the designer. For each particle (i), the position is first chosen by the initialisation technique. The position of all particles is denoted by a vector $x_i(t)$. Moreover, the particles have a velocity represented by a vector $v_i(t)$ with the same

TABLE 2. The details of the PSO algorithm’s operation.

Particle Swarm Optimization Algorithm	
1. Start Procedure	
	Inputs:
	c_1 : Cognitive coefficient
	c_2 : Social coefficient
	NP : Population size
	w : inertia weight
2. Initialise the whole swarm using the Random initialisation technique and evaluate fitness	
3. While ($Ite \leq Ite_{max}$)	
4. Evaluate each particle $f(x_i)$	
5. For ($i=1, i \leq NP, i++$) Do	
6. Update particle velocity:	
	$v_i(t) = w * v_i(t - 1) + c_1 * r_1 * (p_i - x_i(t - 1)) + c_2 * r_2 * (p_g - x_i(t - 1))$
7. Move to new position:	
	$X_i(t) = X_i(t - 1) + v_i(t)$
8. If ($f(x_i) \leq f(p_i)$); then $p_i = x_i$	
9. If ($f(x_i) \leq f(p_g)$); then $p_g = x_i$	
10. Update (x_i, v_i);	
11. End For	
12. End While	
13. Output: Best Solution	
14. End Procedure	

dimension as the position vector. The velocity vector identifies the direction and distance from the current position. Particles collaborate and learn together to reach the optimum solution.

As the particles move and explore the search space, they memorise their personal best solution (p_i) and share it with the rest of the swarm. The best solution among all particles is memorised as the global best (p_g). All the particles update their position and velocity in each iteration using the following operations from A to C.

A. UPDATING THE PARTICLE’S LOCAL AND PERSONAL BEST SOLUTION

The particle’s position is initialised using the initialisation technique. Then, the fitness function of each position is evaluated. This fitness value is initially saved as the personal best; then, it will be compared with fitness values as the particle moves. If the fitness value of the new position is better than the personal best, the new fitness value will be assigned as the personal best, while the old personal best will be deleted, as illustrated in (14). This procedure will be repeated for all particles. The personal bests of all particles will be compared, and the one with the best fitness value will be assigned as the global best, as illustrated in (15).

$$if f(x_i) < p_{best_i}, then p_i = x_i \tag{14}$$

$$\text{if } f(x_i) < g_{best_i}, \text{ then } g_i = x_i \quad (15)$$

B. UPDATING THE PARTICLE'S VELOCITY

The local and global best, along with other factors, are used to identify the particle's velocity, as shown in (16).

$$v_i(t) = w * v_i(t - 1) + c_1 * r_1 * (p_i - x_i(t - 1)) + c_2 * r_2 * (p_g - x_i(t - 1)) \quad (16)$$

The coefficient (w) controls the influence of the previous velocity on the current one, and it is called the inertia coefficient. c_1 and c_2 are learning factors. They represent the influence of personal and global best, respectively. Finally, r_1 and r_2 are uniform random factors ranging from 0 to 1.

C. UPDATING THE PARTICLE'S POSITION

After the position is initiated and the velocity is calculated, the new position is obtained, as shown in (17).

$$x_i(t) = x_i(t - 1) + v_i(t) \quad (17)$$

The details and step-by-step operation of PSO are illustrated in Table 2.

V. CONTROLLING OF THE HYBRID ACTIVE HARMONIC FILTER (HAHF)

The boost converter (EI) is responsible for the harmonic cancellation, ensuring that a square-shaped dc current and regulated output voltage are attained. In order to achieve these goals, a voltage control loop and a fast, reliable, current control loop need to be implemented.

Fig. 9 illustrates the control scheme implemented for the boost converter (EI). In this controller, the desired output voltage (V_o^*) is compared with the measured boosted voltage (V_o), then processed by a Proportional-Integral (PI) controller. The output of the PI controller is multiplied by a modulated signal (M), which contains the optimised parameters (α_f , α_1 , δ , and I_{dc2}) and synchronised with the grid voltage (v_{ab}). The multiplication results in a pulse-shaped reference dc current (I_{LI}^*), which needs to be compared with the measured dc current (I_{LI}). The output of this comparison is sent to a hysteresis band to generate the required switching signal (SW) for the boost converter's switch.

The hysteresis current control loop in Fig. 9 is extremely fast as compared to the voltage control loop; hence, its transfer function can be neglected. On the other hand, the transfer function of the voltage control loop is necessary to choose the proportional and integral gain properly. The transfer function is provided in (18).

$$G_{open-loop} = \frac{v_o(s)}{i_L(s)} = \frac{V_{SCR} \frac{R}{2}}{2V_o(1 + \frac{RC}{2}s)} \quad (18)$$

The SCR's firing angle (α_f) and the boost (EI) switch's switching signal (SW) are the control parameters of the SCR-EI-based HAHF. The switching signal (SW) is controlled to cancel harmonics and produce a square-shaped dc boost or EI's current, as illustrated in Fig. 10, while maintaining a

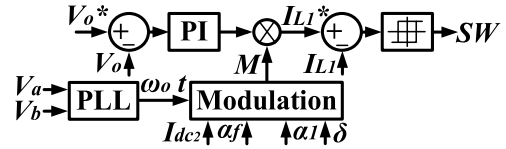


FIGURE 9. The block diagram of the proposed shifted pulse modulation technique.

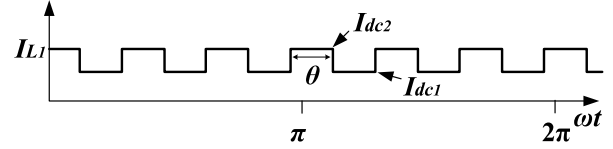


FIGURE 10. The square-shaped EI's dc current.

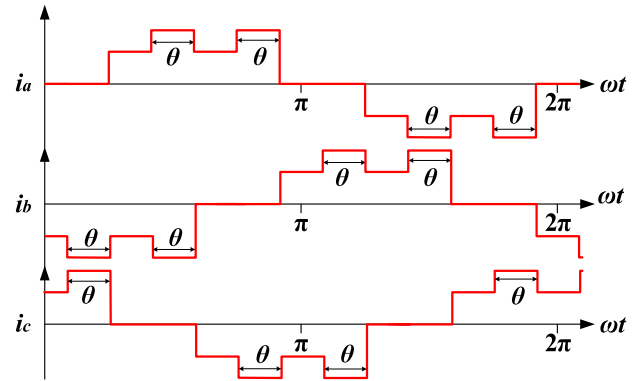


FIGURE 11. The three-phase input currents of the hybrid active harmonic filter (SCR-EI).

regulated boosted output voltage. This current has a periodic waveform with a period of $\pi/3$ to ensure that all phases have identical current waveforms. The width and amplitude of this squared dc current are θ and I_{dc2} , respectively. The parameters of the dc square-shaped current (α_f , α_1 , δ , and I_{dc2}) are optimised by solving (13) using the programmed optimisation algorithm (PSO).

Fig. 11 depicts the three-phase input current of the HAHF. It is obvious that only two phases are simultaneously conducted due to the effect of the three-phase SCR bridge rectifier. Implementing a Phase-Locked Loop (PLL) controller is necessary to synchronise the pulse-shaped dc current, shown in Fig. 10, with the grid voltage.

Moreover, selecting an appropriate inductor value is essential to ensure the operation is in Continuous Conduction Mode (CCM), thus, generating the required square-shaped dc current.

VI. HARDWARE IMPLEMENTATION

The passive component and the controller parameters of the proposed hybrid harmonic filter need to be designed; then, a simulation model is implemented, followed by a hardware implementation to validate the proposed technique.

Fig 12 illustrates the implemented prototype for the hybrid active harmonic filter (HAHF) system, similar to the proposed system in Fig. 3. An auto-transformer (Variac) is utilised to reduce the grid voltage to 110V.

The practical setup consists of two main parallel stages. The first stage is the Single Drive System represented by a conventional 3-phase Diode Rectifier (DR) with a passive filter. The second stage is the Hybrid Active Harmonic Filter (HAHF), which is the Silicon Controlled Rectifier (SCR) integrated with a boost-based Electronic Inductor (EI).

The conventional DR with a passive filter is implemented to represent the ASD distribution network. A SEMIKRON-SKD 30 three-phase diode rectifier is employed. The passive filter's inductor and capacitor values are 6 mH and 235 μ F, respectively.

For the HAHF, an SK 70 DT three-phase SCR bridge is employed, while a driver circuit, named FC36M, is employed to drive the SCR bridge. The integrated boost-based EI employed a SEMIKRON-SKM75 Insulated-Gate Bipolar Transistor (IGBT), inductor, and capacitor values of 2 mH and 560 μ F, respectively. The EI's IGBT is derived by a SKYPER_32_R gate driver. Two 1kW resistive loads are utilised for the DR and the SCR-EI.

A PLL circuit utilised to synchronise the HAHF or SCR-EI's pulse-shaped current with the grid voltage. The control loops of the boost converter are implemented in a Texas Instrument F28379D microcontroller.

Current and voltage probs are used for controlling and measurement purposes. The current peak-to-peak ripple is 1.5 A, the average inductor current is 3.5 A, the switching frequency is 12 kHz, and the system's rated power is 1 kW.

VII. RESULTS

The system with two units is implemented with a configuration as shown in Fig. 3. An ASD with a front-end DR with a passive filter is considered as a case study of grid harmonics, while an SRC-EI is proposed as a hybrid active harmonic filter. The goal of this research is to minimise the major harmonics (5th, 7th, 11th, and 13th) produced by the first unit (conventional DR).

A shifted pulse modulation method for the SCR-EI is proposed to generate harmonics in the opposite phase of the ones in the DR. To validate the proposed method, a simulation model and a practical setup are implemented. The test parameters are shown in Table 3. The system is tested for two cases.

1) CASE I IS WHEN THE HAHF PRODUCES AN UNMODULATED CURRENT (FLAT CURRENT WAVEFORM).

2) CASE II IS WHEN THE HARMONIC FILTER PRODUCES THE OPTIMAL PULSE-SHAPED CURRENT (MODULATED).

A. SIMULATION RESULTS

A 1kW MATLAB/Simulink model is built. The parameters of this model are illustrated in Table 3. The major harmonics magnitudes and phase angles for the DR operating at full power operation are shown in Table 1. The optimisation algorithm (PSO) is employed to produce a current waveform that has harmonics with opposite phase angles as the ones caused by the front-end DR.

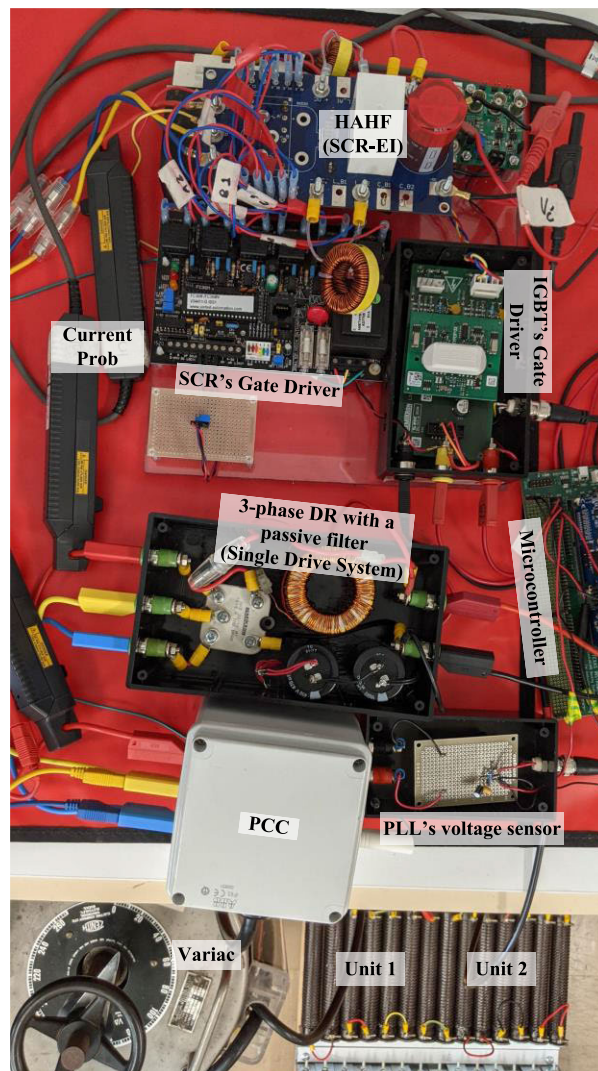


FIGURE 12. The practical setup of DR and SCR-EI.

TABLE 3. The system's parameters.

System parameters	Symbol	Value
Grid Voltage	$V_{a,b,c}$	110V
Grid Frequency	f_s	50 Hz
Passive filters Inductance	L_d	6 mH
Passive filters Capacitance	C_d	225 μ F
SCR-EI's dc-link Voltage	V_o	320V
EI's Inductance	L_1	2 mH
Stray Resistor of Inductor	R_L	0.1 Ω
SCR-EI's Capacitance	C_1	590 μ F
Load Resistor	R	160 Ω
Output power	P_o	800 W
Proportional, Integral gain	K_i, K_p	0.1, 5
Hysteresis band	H_b	0.75 A

The results of the PSO algorithm for the full power operation is depicted in Table 4. When the optimised parameters are applied in the simulation model, the current THD significantly reduces.

TABLE 4. The results of the PSO algorithm.

PSO results	Firing angle (α_f)	Pulse's magnitude (I_{dc2})	Pulse starting point (α_r)	Pulse's shift (δ)
Full power	38.008°	-0.700	49.307°	-19.307°

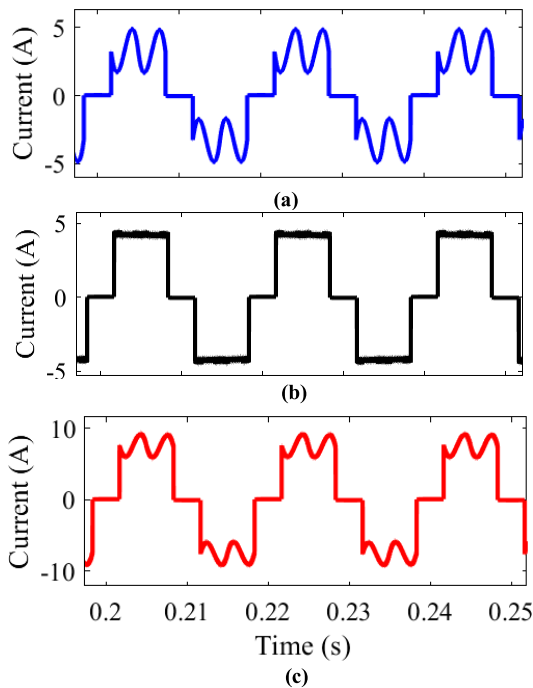


FIGURE 13. (a) The phase current drawn by a DR with the passive filter operating at full power (b) The flat square-shaped phase current drawn by the SCR-EI filter without modulation (c) The total phase current drawn from the mains when the SCR-EI filter is employed in parallel with DR.

Fig. 13 shows the phase current waveforms of case I. The phase current of the DR operating at 100% load is depicted in Fig. 13 (a). A flat phase current waveform (without harmonic cancellation) drawn by the HAHF (SCR-EI) is illustrated in Fig. 13 (b), while Fig. 13 (c) shows the total phase current drawn from the mains when the SCR-EI is employed in parallel with front-end DR.

A comparison between the harmonics generated by the waveform in Fig. 13 (a) and the waveform in Fig. 13 (c) is demonstrated in Fig. 14. It is illustrated in Fig.14 that the 5th harmonic is reduced from 36.1% to 24.2%, while the 7th harmonic decreased from 26.5% to 17.5%. The 11th harmonic is increased slightly, while the 13th has a slight reduction.

Fig. 15 presents the phase current waveforms of Case II. The phase current drawn from the grid when the DR is operating at full power is depicted in Fig. 15 (a). When the shape of the SCR-EI's current waveform is optimised, it draws a current waveform, as illustrated in Fig. 15 (b). Hence, the total current drawn from the mains has significantly improved, as illustrated in Fig. 15 (c). The harmonic contents of the waveforms in Fig. 15 (a) and Fig. 15 (c) are compared in Fig. 16. The comparison illustrates that the 5th, 7th

TABLE 5. Comparison of harmonics contents of the proposed method with methods presented in [39].

Harmonics mitigation method	THDi and Harmonics content of grid current				
	THDi	5 th	7 th	11 th	13 th
Conventional Units (Case I)	34.2	24.2	17.5	9.2	7.7
Method presented in [39]	36	32	1	9	8
Proposed Method	17	4.7	10.1	3.2	7.7

and 11th harmonics significantly reduce from 36.1%, 26.5%, and 8.9% to 4.7%, 10.1%, and 3.2%, respectively. On the other hand, the 13th harmonic has a slight reduction from 8.4% to 7.7%.

Table 5 presents a detailed comparison of THDi and harmonics contents for the proposed method with the methods presented in the literature [39]. The method proposed in [39] is based on employing the shifted pulse method on DR to mitigate a specific harmonic from the grid.

In contrast, the proposed method is based on SCR to further mitigate multi-grid harmonics and reduce the grid THDi. Hence, Table 5 indicates that the proposed method has a lower grid THDi with only 17% compared to 36% of the method proposed in [39]. The proposed method is superior to the method proposed in [39] in terms of the total harmonic distortions and the fifth, eleventh, and thirteenth harmonics. However, since the method proposed in [39] targets a specific harmonic order, the seventh harmonics are lower than the one in the proposed method.

Moreover, the results from the table show that the proposed method significantly reduces the grid harmonics content and THDi compared to the conventional system (case I). The simulation results demonstrate that employing the proposed HAHF reduces the THDi value significantly. In fact, employing the proposed SCR-EI-based HAHF with an optimised current waveform allows a wider range of current harmonics to be mitigated as compared to the pre-existing DR-EI-based harmonic filter [39].

The existing DR-EI-based filter reduces the THDi from 48% to 36%, whereas the proposed method (with HAHF) reduces the THDi from 48% to 17%.

B. PRACTICAL VALIDATIONS

A 1kW prototype, consisting of a front-end DR with a passive filter and parallel SCR-EI HAHF, has been implemented in the laboratory to validate the proposed harmonic mitigation method, as shown in Fig. 12.

The parameters of the prototype are shown in Table 3. Similar to simulation results, two cases have been carried out in the practical tests.

Fig. 17 (a) depicts the phase currents of the DR at full-power operation (blue waveform), HAHF (green waveform), and total main's current (yellow waveform) in Case I, where the HAHF generates a flat dc current (without harmonic cancellation).

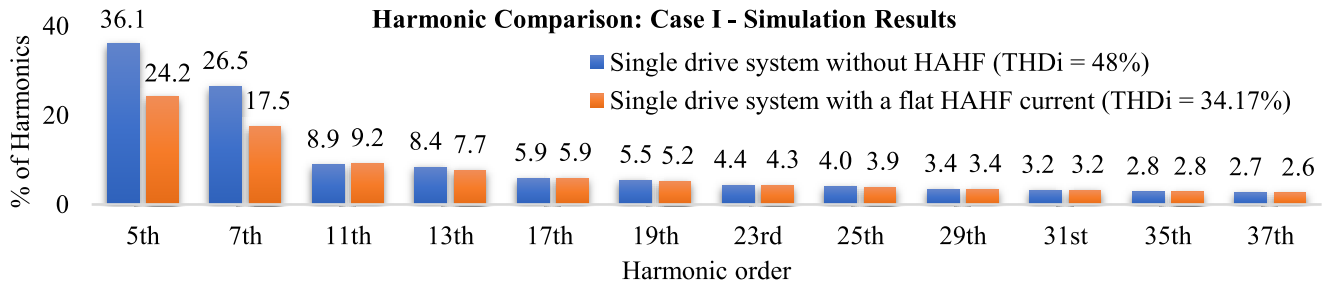


FIGURE 14. Harmonic contents of the simulated DR and mains phase currents in Case I.

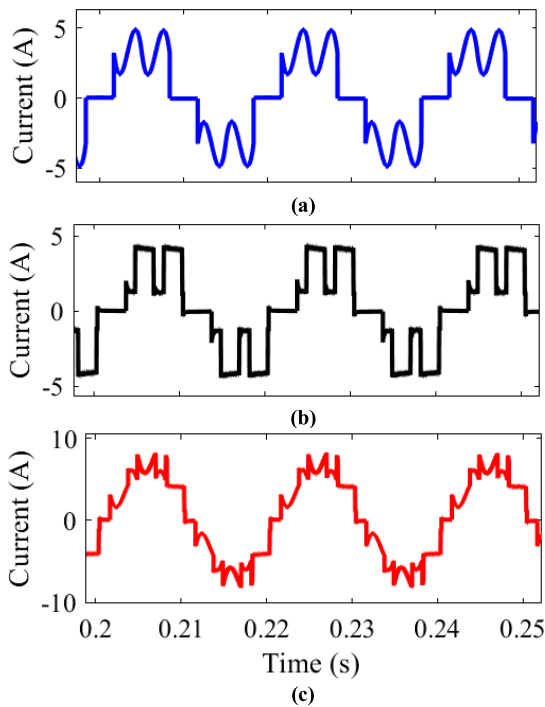


FIGURE 15. (a) The phase current drawn by a DR with the passive filter operating at full power (b) The optimised phase current drawn by the SCR-EI filter to mitigate the harmonics generated by DR (c) The total phase current drawn from the mains when the SCR-EI filter is employed in parallel with DR.

A comparison between the harmonics produced by the front-end DR and the total harmonics when the SCR-EI generates a flat-shaped current is demonstrated in Fig. 18.

The results in Fig. 18 illustrate that the 5th, 7th, 11th, and 13th harmonics have reduced from 40.6%, 22.7%, 8.7%, and 5.1% to 30.8%, 10.2%, 7.2%, and 4.3% when the SCR-EI filter generates flat dc current. In addition, the total harmonics (THDi) is decreased from 48.28% to 34.34%.

Fig. 13 and 17 (a) illustrate both the simulation and practical results, respectively, when the HAHF produces an unoptimized square shape waveform. The figures show the current waveforms of the distribution network (represented by the front-end DR), the HAHF, and the total current drawn from the PCC. The simulation and practical waveforms, in Fig. 13 and 17 (a), are analysed in both Fig. 14 and Fig. 18.

The harmonic contents of the single ASD system in the practical results have 4.5%, 3.8%, 0.2%, and 3.3% difference in the 5th, 7th, 11th, and 13th harmonics, while the THDi is 0.28% higher in the practical results as compared to the simulation results. On the other hand, the harmonic contents of the total current of the system have a difference of 6.6%, 7.3%, 2%, and 3.4% in the 5th, 7th, 11th, and 13th harmonics, while the THDi has a difference of 0.17% between simulation and practical results.

In Fig. 17 (b), the phase current waveform of the DR at full power is shown in blue colour. The waveform in green represents the optimised pulse-shaped current generated by the HAHF using the parameters in Table 4. Finally, the system’s total phase current is represented in yellow colour.

A comparison of harmonic contents generation between the utilisation of conventional DR and employing a HAHF in parallel with the DR is depicted in Fig. 19. Similar to the simulation results, the comparison in Fig. 19 demonstrates that the utilisation of the HAHF results in a significant reduction in the 5th and 7th harmonics from 40.6% and 22.7% to 4.5% and 9.2%. The 11th harmonic has a slight reduction from 8.7% to 5.2%, while the 13th harmonic has a slight increase from 5.1% to 5.4%. In addition, the total harmonics (THDi) is reduced from 48.28% to 15.07%.

According to the harmonic analysis figures (Fig. 16 and Fig. 19), the practical results validate the simulation results, but the harmonic contents are slightly different. For instance, the harmonic contents of the total current (After using HAHF) have a difference of 0.2%, 0.9%, 2%, and 2.3% in the 5th, 7th, 11th, and 13th harmonics, and the THDi is 2% less in the practical results as compared to the simulation results due to several factors, such as lossy elements, stray parameters, control design, and dynamic performance of the current, measuring system, and noises.

To sum up, the proposed current harmonics mitigation method is validated by both simulation and practical results. Moreover, the proposed method results in superior performance as compared to the literature [39]. The proposed filter has improved the THDi of the mains’ current from 48% to 15%.

C. POWER RATING, COST, AND LOSSES CALCULATION

The system used to implement the proposed method is based on two units rated at 800 W each. This was a prototype

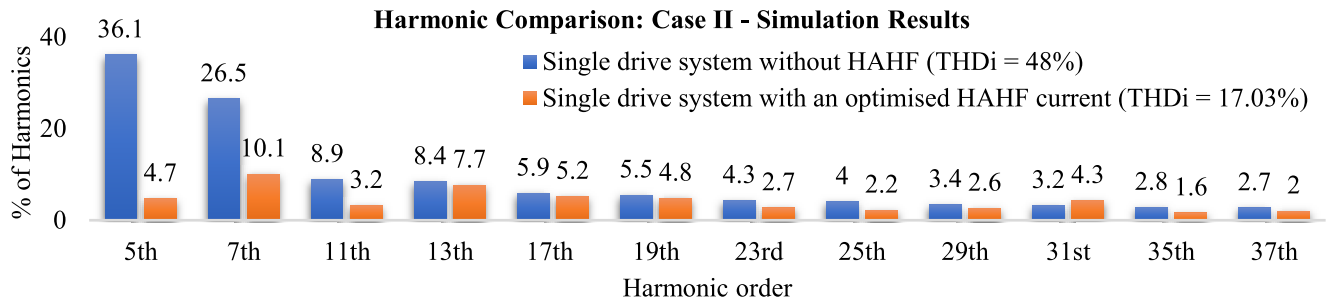


FIGURE 16. Harmonic contents of the simulated DR and mains phase currents in Case II.

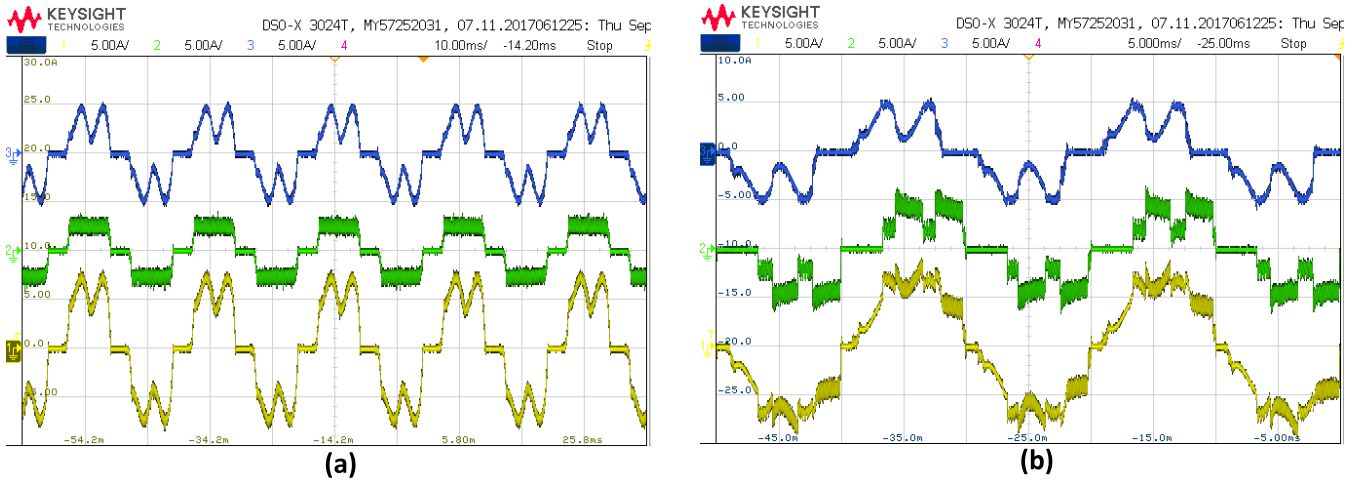


FIGURE 17. (a) The phase currents in the time domain for Case I, HAHF is generating flat dc current. (b) The phase currents in the time domain for Case II, HAHF is generating a pulse-shaped current.

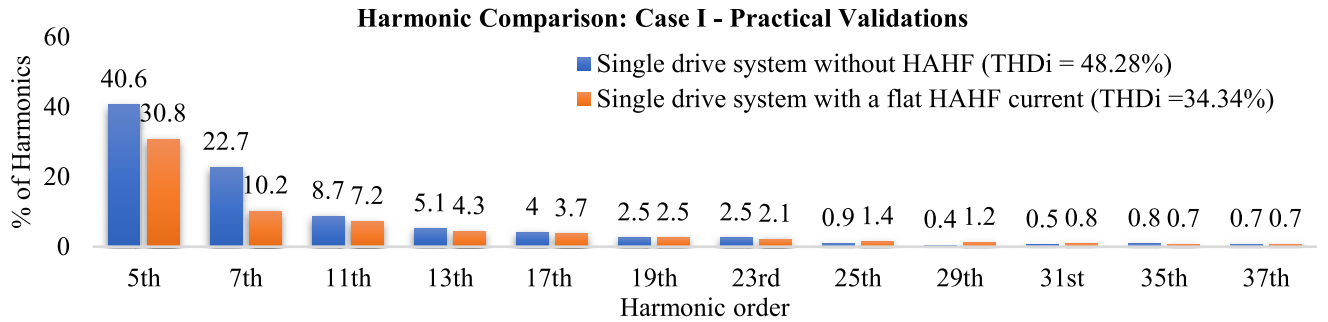


FIGURE 18. Harmonic contents of the practical DR and mains phase currents in Case I.

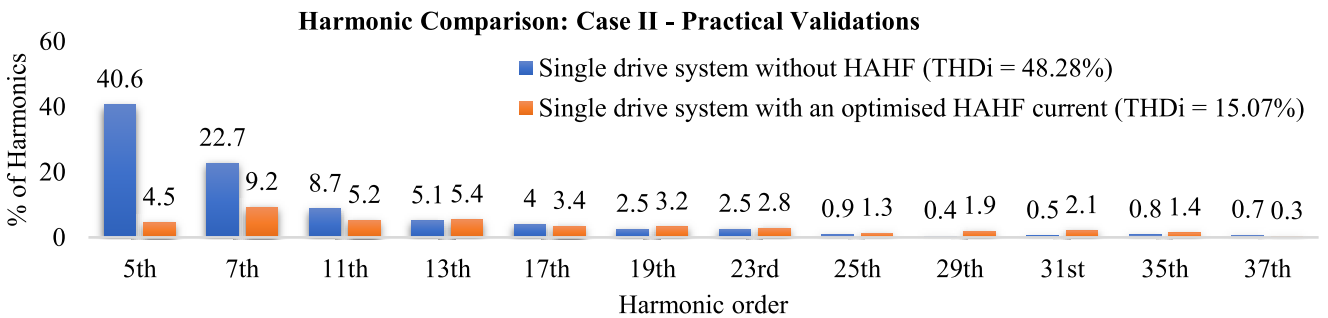


FIGURE 19. Harmonic contents of the practical DR and mains phase currents in Case II.

to validate the proposed method. However, the target of this method is to be implemented on ASDs with a medium power rating (16 -75 Amps), which complies with IEC 61000-3-12 [29]. The utilization of these types of drives is common on commercial and industrial networks. Three-phase SCR (or DR) with intermediate circuits are common topologies used as a front-end due to their reliability, control simplicity, and cost-effectiveness. The cost of SCR-EI compared to an active front-end is much lower due to the reduction of active switches. The losses of the power converter are mainly determined by the number of switches, switching material, switching frequency, and power rating of the converter. Therefore, the losses alter when the ASD system operates at partial power. A comprehensive study about EI losses has been discussed in [44]. The efficiency of an SCR front-end topology with EI when it operates at full power is 96%.

VIII. CONCLUSION

In this paper, a modified pulse-shaped current for a Hybrid Active Harmonic Filter (HAHF) is proposed. The HAHF is based on a Silicon-Controlled Rectifier (SCR) with an integrated Electronic Inductor (EI). The dc current of the boost-based EI is controlled to generate a pulse-shaped current and minimise the grid's harmonics. The parameters of the pulse-shaped current (magnitude, width, and starting point) are optimised using Particle Swarm Optimisation (PSO) algorithm to mitigate harmonic from the grid. The proposed technique has the capability to control the harmonics at the PCC. In addition, it significantly reduces the current Total Harmonic Distortion (THD_i) generated at the PCC. An electrical distribution network with Single Drive System is selected as a case study. The validity of the proposed technique is proved by a MATLAB/Simulink model and a 1 kW practical setup. The system is tested in two cases; the first case is when the HAHF draws a simple square waveform, while case two is when the HAHF draws an optimised pulse-shaped current. The HAHF reduced the electrical grid's 5th, 7th, 11th, and 13th harmonic contents from 36.1%, 26.5%, 8.9%, and 8.4 to 4.7%, 10.1%, 3.2%, and 7.7%, respectively. In addition, the THD_i is reduced from 48% to 17.03%. The results prove that the proposed method significantly improves the power quality of the electrical distribution network. The proposed harmonic mitigation technique is suitable for commercial and industrial distribution networks.

REFERENCES

- [1] A. Emadi, A. Z. Khaligh Nie, and Y. J. Lee, *Integrated Power Electronic Converters and Digital Control*, 1st ed. Boca Raton, FL, USA: CRC Press, 2017, pp. 31–36.
- [2] *IEEE Recommended Practice and Requirements for Harmonic Control in Electric Power Systems*, Standard 519–2014 (Revision of IEEE Std 519–1992), IEEE, Jun. 2014, pp. 1–29.
- [3] S. Martinius, B. Halimi, and P. A. Dahono, "A transformer connection for multipulse rectifier applications," in *Proc. Int. Conf. Power Syst. Technol.*, 2002, pp. 1021–1024.
- [4] S. Choi, N. E. Prasad, and I. J. Pitel, "Polyphase transformer arrangements with reduced kVA capacities for harmonic current reduction in rectifier-type utility interface," *IEEE Trans. Power Electron.*, vol. 11, no. 5, pp. 680–690, Sep. 1996.
- [5] R. K. Girish, D. Benson, and R. Wood, "A novel autotransformer based 18-pulse rectifier circuit," in *Proc. IEEE APEC*, Mar. 2002, pp. 795–801.
- [6] B. Singh, G. Bhuvaneswari, and V. Garg, "An improved power-quality 30-pulse AC–DC for varying loads," *IEEE Trans. Power Del.*, vol. 22, no. 2, pp. 1179–1187, Apr. 2007.
- [7] F. Zare, "Modular multi-parallel rectifiers (MMR) with two DC link current sensors," in *Proc. IEEE Energy Convers. Congr. Expo. (ECCE)*, Milwaukee, WI, USA, Sep. 2016, pp. 1–7.
- [8] A. Sunbul, F. Zare, R. Sharma, and A. Ghosh, "Democratic current sharing controller for modular multi-parallel rectifiers (MMR)," in *Proc. 31st Australas. Universities Power Eng. Conf. (AUPEC)*, Sep. 2021, pp. 1–6.
- [9] J. W. Kolar and T. Friedli, "The essence of three-phase PFC rectifier systems—Part I," *IEEE Trans. Power Electron.*, vol. 28, no. 1, pp. 176–198, Jan. 2013.
- [10] K. Schipman and F. Delince, "The importance of good power quality," ABB Rev., ABB Power Qual. Prod., Charleroi, Belgium, Tech. Rep. 1, Apr. 2010.
- [11] H. Hu, W. Shi, Y. Lu, and Y. Xing, "Design considerations for DSP-controlled 400 Hz shunt active power filter in an aircraft power system," *IEEE Trans. Ind. Electron.*, vol. 59, no. 9, pp. 3624–3634, Sep. 2012.
- [12] J. Liu, P. Zanchetta, M. Degano, and E. Lavopa, "Control design and implementation for high performance shunt active filters in aircraft power grids," *IEEE Trans. Ind. Electron.*, vol. 59, no. 9, pp. 3604–3613, Sep. 2012.
- [13] W.-H. Ko and J.-C. Gu, "Impact of shunt active harmonic filter on harmonic current distortion of voltage source inverter-fed drives," *IEEE Trans. Ind. Appl.*, vol. 52, no. 4, pp. 2816–2825, Jul. 2016.
- [14] R. Pandurangan, P. Kaliannan, and P. Shanmugam, "Effects of current distortion on DC link inductor and capacitor lifetime in variable frequency drive connected to grid with active harmonic filter," *IEEE Trans. Ind. Appl.*, vol. 57, no. 1, pp. 492–505, Jan. 2021.
- [15] Y. Tang, P. C. Loh, P. Wang, F. H. Choo, F. Gao, and F. Blaabjerg, "Generalized design of high performance shunt active power filter with output LCL filter," *IEEE Trans. Ind. Electron.*, vol. 59, no. 3, pp. 1443–1452, Mar. 2012.
- [16] J. Tian, Q. Chen, and B. Xie, "Series hybrid active power filter based on controllable harmonic impedance," *IET Power Electron.*, vol. 5, no. 1, pp. 142–148, 2012.
- [17] S. Rahmani, A. Hamadi, K. Al-Haddad, and A. I. Alolah, "A DSP-based implementation of an instantaneous current control for a three-phase shunt hybrid power filter," *Math. Comput. Simul.*, vol. 91, pp. 229–248, May 2013.
- [18] C.-S. Lam, W.-H. Choi, M.-C. Wong, and Y.-D. Han, "Adaptive DC-link voltage-controlled hybrid active power filters for reactive power compensation," *IEEE Trans. Power Electron.*, vol. 27, no. 4, pp. 1758–1772, Apr. 2012.
- [19] A. Bhattacharya, C. Chakraborty, and S. Bhattacharya, "Parallel-connected shunt hybrid active power filters operating at different switching frequencies for improved performance," *IEEE Trans. Ind. Electron.*, vol. 59, no. 11, pp. 4007–4019, Nov. 2012.
- [20] B. Singh, V. Verma, A. Chandra, and K. Al-Haddad, "Hybrid filters for power quality improvement," *IEE Proc. Gener., Transmiss. Distrib.*, vol. 152, no. 3, pp. 365–378, May 2005.
- [21] F. D. Freijedo, J. Doval-Gandoy, Ó. Lopez, P. Fernandez-Comesana, and C. Martinez-Penalver, "A signal-processing adaptive algorithm for selective current harmonic cancellation in active power filters," *IEEE Trans. Ind. Electron.*, vol. 56, no. 8, pp. 2829–2840, Aug. 2009.
- [22] S. Rahmani, A. Hamadi, N. Mendalek, and K. Al-Haddad, "A new control technique for three-phase shunt hybrid power filter," *IEEE Trans. Ind. Electron.*, vol. 56, no. 8, pp. 2904–2915, Aug. 2009.
- [23] A. Hamadi, S. Rahmani, and K. Al-Haddad, "Digital control of a shunt hybrid power filter adopting a nonlinear control approach," *IEEE Trans. Ind. Informat.*, vol. 9, no. 4, pp. 2092–2104, Nov. 2013.
- [24] R. Inzunza and H. Akagi, "A 6.6-kV transformerless shunt hybrid active filter for installation on a power distribution system," *IEEE Trans. Power Electron.*, vol. 20, no. 4, pp. 893–900, Jul. 2005.
- [25] L. R. Limongi, L. R. da Silva Filho, L. G. B. Genu, F. Bradaschia, and M. C. Cavalcanti, "Transformerless hybrid power filter based on a six-switch two-leg inverter for improved harmonic compensation performance," *IEEE Trans. Ind. Electron.*, vol. 62, no. 1, pp. 40–51, Jan. 2015.
- [26] J.-C. Wu, H. L. Jou, Y.-T. Feng, W.-P. Hsu, M.-S. Huang, and W.-J. Hou, "Novel circuit topology for three-phase active power filter," *IEEE Trans. Power Del.*, vol. 22, no. 1, pp. 444–449, Jan. 2007.

- [27] W. U. K. Tareen and S. Mekhief, "Three-phase transformerless shunt active power filter with reduced switch count for harmonic compensation in grid-connected applications," *IEEE Trans. Power Electron.*, vol. 33, no. 6, pp. 4868–4881, Jun. 2018.
- [28] J. E. Hernandez, R. P. Kandula, F. C. Lambert, and D. Divan, "A practical directional third harmonic hybrid active filter for medium-voltage utility applications," *IEEE Trans. Ind. Appl.*, vol. 49, no. 6, pp. 2674–2683, Nov. 2013.
- [29] *Electromagnetic Compatibility (EMC)—Part 3–12: Limits—Limits for Harmonic Currents Produced by Equipment Connected to Public Low-voltage Systems With Input Current >16 A and ≤75 A Per Phase*, Standard IEC 61000–3–12, 2011.
- [30] H. Ertl and J. W. Kolar, "A constant output current three-phase diode bridge rectifier employing a novel electronic smoothing Inductor," *IEEE Trans. Ind. Electron.*, vol. 52, no. 2, pp. 454–461, Apr. 2005.
- [31] F. Zare, "A novel harmonic elimination method for a three-phase diode rectifier with controlled DC link current," in *Proc. 16th Int. Power Electron. Motion Control Conf. Expo.*, Antalya, Turkey, Sep. 2014, pp. 985–989.
- [32] P. Davari, F. Zare, and F. Blaabjerg, "Pulse pattern-modulated strategy for harmonic current components reduction in three-phase AC–DC converters," *IEEE Trans. Ind. Appl.*, vol. 52, no. 4, pp. 3182–3192, Aug. 2016.
- [33] A. Alduraibi, J. Yaghoobi, H. Rathnayake, F. Zare, and R. Sharma, "Dynamic analysis of a modular three-phase rectifier system with harmonic mitigation function: Addressing IEC 61000–3–12," in *Proc. IEEE Int. Conf. Ind. Technol. (ICIT)*, Feb. 2019, pp. 1235–1240.
- [34] A. Alduraibi, J. Yaghoobi, D. Solatalkaran, and F. Zare, "A modular power converter with active front-end system to mitigate harmonics in distribution networks," *IEEE J. Emerg. Sel. Topics Power Electron.*, vol. 9, no. 2, pp. 1725–1735, Apr. 2021.
- [35] A. Alduraibi, J. Yaghoobi, F. Zare, and R. Sharma, "A new technology to reduce harmonic emission in distribution networks: Addressing IEC 61000–3–12," in *Proc. Australas. Universities Power Eng. Conf. (AUPEC)*, Nov. 2018, pp. 1–6.
- [36] P. Davari, Y. Yang, F. Zare, and F. Blaabjerg, "A multipulse pattern modulation scheme for harmonic mitigation in three-phase multimotor drives," *IEEE J. Emerg. Sel. Topics Power Electron.*, vol. 4, no. 1, pp. 174–185, Mar. 2016.
- [37] F. Zare, P. Davari, and F. Blaabjerg, "A modular active front-end rectifier with electronic phase shifting for harmonic mitigation in motor drive applications," *IEEE Trans. Ind. Appl.*, vol. 53, no. 6, pp. 5440–5450, Jul. 2017.
- [38] Y. Yang, P. Davari, F. Blaabjerg, and F. Zare, "Load-independent harmonic mitigation in SCR-fed three-phase multiple adjustable speed drive systems with deliberately dispatched firing angles," *IET Power Electron.*, vol. 11, no. 4, pp. 727–734, Apr. 2018.
- [39] A. Alduraibi, J. Yaghoobi, D. Solatalkaran, F. Zare, and R. Sharma, "Harmonic mitigation technique using active three-phase converters utilised in commercial or industrial distribution networks," *IET Power Electron.*, vol. 13, no. 13, pp. 2794–2803, Oct. 2020.
- [40] R. Gou, "Research on 1100-kV/5500-A ultra-high voltage thyristor valve key technology and its application," *IEEE Trans. Power Electron.*, vol. 34, no. 11, pp. 10524–10533, Nov. 2019.
- [41] J. Titus, H. P. and K. Hatua, "An SCR-based CSI-fed induction motor drive for high power medium voltage applications," *IEEE Trans. Ind. Electron.*, vol. 68, no. 6, pp. 4657–4666, Jun. 2021.
- [42] X. Jin and H. Nian, "Overvoltage suppression strategy for sending AC grid with high penetration of wind power in the LCC-HVdc system under commutation failure," *IEEE Trans. Power Electron.*, vol. 36, no. 9, pp. 10265–10277, Sep. 2021.
- [43] F. Khan, A. Sunbul, M. Y. Ali, H. Abdei-Gawad, S. Rahnamayan, and V. K. Sood, "Maximum power point tracking in photovoltaic farms using DE and PSO algorithms: A comparative study," in *Proc. IEEE Congr. Evol. Comput. (CEC)*, Jul. 2018, pp. 1–9.
- [44] P. Davari, Y. Yang, F. Zare, and F. Blaabjerg, "A review of electronic inductor technique for power factor correction in three-phase adjustable speed drives," in *Proc. IEEE Energy Convers. Congr. Expo. (ECCE)*, Sep. 2016, pp. 1–8.



ALI SUNBUL (Student Member, IEEE) was born in Saudi Arabia. He received the B.S. and M.S. degrees in electrical engineering from the University of Ontario Institute of Technology (Ontario Tech), Oshawa, ON, Canada, in 2016 and 2019, respectively. He is currently pursuing the Ph.D. degree in electrical engineering with The University of Queensland (UQ), Brisbane, QLD, Australia.

Since 2017, he has been a Lecturer at Taibah University, Yanbu, Medina, Saudi Arabia. His research interests include modeling and control of power electronic systems, and power quality.



ABDULRAHMAN ALDURAIBI (Member, IEEE) received the B.Sc. degree in electrical engineering from Qassim University, Buraydah, Saudi Arabia, in 2010, the M.Sc. degree in electrical engineering from The George Washington University, Washington, DC, USA, in 2017, and the Ph.D. degree in power electronics from The University of Queensland (UQ), Brisbane, QLD, Australia, in 2021. From 2010 to 2013, he was a Testing and Commissioning Engineer with ABB, Riyadh, Saudi Arabia. He is currently an Assistance Professor with the Department of Electrical Engineering, College of Engineering, Qassim University, Unaizah, Saudi Arabia. His research interests include power electronics, power quality, and power converters.



FIRUZ ZARE (Fellow, IEEE) received the Ph.D. degree in power electronics from the Queensland University of Technology, Australia, in 2002.

He has over 20 years of experience in academia, industry, and international standardization committees, including eight years in two large research and development centers working on power electronics and power quality projects. He is currently a Power Electronics Professor and the Head of the School of Electrical Engineering and Robotics, Queensland University of Technology. He is also the Task Force Leader (International Project Manager) of Active Infeed Converters to develop the first international standard IEC 61000-3-16 within the IEC standardization SC77A. He has published four books, over 280 journal articles and conference papers, five patents, and over 40 technical reports. His main research interests include power electronics topology, control and applications, power quality and regulations, and pulsed power applications.

Prof. Zare has received several awards, such as the Australian Future Fellowship, the John Madsen Medal, the Symposium Fellowship, and the Early Career Excellence Research Award. He is a Senior Editor of IEEE ACCESS journal, a Guest Editor and an Associate Editor of the IEEE JOURNAL OF EMERGING AND SELECTED TOPICS IN POWER ELECTRONICS, an Associate Editor of IET Journal, and an editorial board member of several international journals.

• • •